AFRL-RX-WP-TP-2012-0352

SIGNAL PROCESSING AND IMAGING WITH ULTRASONIC GUIDED WAVES: GOALS, CHALLENGES AND RECENT PROGRESS (PREPRINT)

Jennifer E. Michaels and Thomas E. Michaels

Georgia Institute of Technology

July 2012
Interim

AIR FORCE RESEARCH LABORATORY
MATERIALS AND MANUFACTURING DIRECTORATE
WRIGHT-PATTERSON AIR FORCE BASE, OH 45433-7750
AIR FORCE MATERIEL COMMAND
UNITED STATES AIR FORCE

REPORT DOCUMENTATION PAGE

Form Approved
OMB No. 0704-0188

1. REPORT DATE *(DD-MM-YY)*	2. REPORT TYPE	3. DATES COVERED *(From - To)*
July 2012	Technical Paper	1 June 2012 – 1 July 2012

4. TITLE AND SUBTITLE
SIGNAL PROCESSING AND IMAGING WITH ULTRASONIC GUIDED WAVES: GOALS, CHALLENGES AND RECENT PROGRESS (PREPRINT)

5a. CONTRACT NUMBER
FA8650-09-C-5206

5b. GRANT NUMBER

5c. PROGRAM ELEMENT NUMBER
62102F

6. AUTHOR(S)
Jennifer E. Michaels and Thomas E. Michaels

5d. PROJECT NUMBER
4349

5e. TASK NUMBER
41

5f. WORK UNIT NUMBER
LP106300

7. PERFORMING ORGANIZATION NAME(S) AND ADDRESS(ES)
Georgia Institute of Technology
Georgia Tech Research Group
505 10th Street NW
Atlanta, GA 30332

8. PERFORMING ORGANIZATION REPORT NUMBER
AFRL-RX-WP-TP-2012-0352

9. SPONSORING/MONITORING AGENCY NAME(S) AND ADDRESS(ES)
Air Force Research Laboratory
Materials and Manufacturing Directorate
Wright-Patterson Air Force Base, OH 45433-7750
Air Force Materiel Command
United States Air Force

10. SPONSORING/MONITORING AGENCY ACRONYM(S)
AFRL/RXCA

11. SPONSORING/MONITORING AGENCY REPORT NUMBER(S)
AFRL-RX-WP-TP-2012-0352

12. DISTRIBUTION/AVAILABILITY STATEMENT
Approved for public release; distribution unlimited. Preprint to be submitted to 18th World Conference on NDT.

13. SUPPLEMENTARY NOTES
This work was funded in whole or in part by Department of Air Force contract FA8650-09-C-5206. The U.S. Government has for itself and others acting on its behalf an unlimited, paid-up, nonexclusive, irrevocable worldwide license to use, modify, reproduce, release, perform, display, or disclose the work by or on behalf of the U.S. Government. PA Case Number and clearance date: 88ABW-2012-1621, 22 March 2012. This document contains color.

14. ABSTRACT
Ultrasonic guided waves have the potential for both rapid inspection and in situ monitoring of plate-like structures, and effective signal processing and imaging algorithms are essential to achieve necessary performance. Although guided waves can propagate long distances and still remain sensitive to damage, their dispersive nature and sensitivity to varying environmental and operational conditions offer significant challenges. This paper addresses two guided wave applications that have recently been the subject of significant research. The first is acquisition and analysis of full or partial guided wavefield data such as can be obtained by either a scanning laser vibrometer or a scanned air-coupled transducer. This application is motivated by the need for a rapid alternative to traditional bulk wave inspections that does not require extensive teardown or liquid couplants. The second is in situ monitoring using a spatially distributed array of simple piezoelectric transducers. This application is motivated by the need for long term monitoring of critical structures to both lower maintenance costs and prevent catastrophic failures.

15. SUBJECT TERMS
lamb waves, wavefield imaging, sparse arrays, adaptive imaging, damage characterization

16. SECURITY CLASSIFICATION OF:			17. LIMITATION OF ABSTRACT:	NUMBER OF PAGES	19a. NAME OF RESPONSIBLE PERSON (Monitor)
a. REPORT	b. ABSTRACT	c. THIS PAGE			Charles Buynak
Unclassified	Unclassified	Unclassified	SAR	12	19b. TELEPHONE NUMBER *(Include Area Code)* N/A

18th World Conference on Nondestructive Testing, 16-20 April 2012, Durban, South Africa

Signal Processing and Imaging with Ultrasonic Guided Waves: Goals, Challenges and Recent Progress

Jennifer E. MICHAELS [1] and Thomas E. MICHAELS [2]

School of Electrical and Computer Engineering, Georgia Institute of Technology,
Atlanta, Georgia, 30332-0250, USA
[1] Phone: 001-404-894-2994, Fax: 001-404-894-4641; e-mail: jennifer.michaels@ece.gatech.edu
[2] e-mail: thomas.michaels@ece.gatech.edu

Abstract
Ultrasonic guided waves have the potential for both rapid inspection and *in situ* monitoring of plate-like structures, and effective signal processing and imaging algorithms are essential to achieve necessary performance. Although guided waves can propagate long distances and still remain sensitive to damage, their dispersive nature and sensitivity to varying environmental and operational conditions offer significant challenges. This paper addresses two guided wave applications that have recently been the subject of significant research. The first is acquisition and analysis of full or partial guided wavefield data such as can be obtained by either a scanning laser vibrometer or a scanned air-coupled transducer. This application is motivated by the need for a rapid alternative to traditional bulk wave inspections that does not require extensive teardown or liquid couplants. The second is *in situ* monitoring using a spatially distributed array of simple piezoelectric transducers. This application is motivated by the need for long term monitoring of critical structures to both lower maintenance costs and prevent catastrophic failures. Recent results are presented from current and past projects of the QUEST Laboratory at Georgia Tech.

Keywords: Lamb waves, wavefield imaging, sparse arrays, adaptive imaging, damage characterization

1. Introduction

Ultrasonic guided waves, which are formed by the interaction of shear and longitudinal bulk waves with structural boundaries, can travel long distances while maintaining sufficient amplitude for damage detection. Guided waves in pipes have been successfully deployed for long distance detection of damage, enabling very fast screening of piping for damage without expensive disassembly [1,2]. One of the reasons for this success is that a pipe supports a wave mode traveling in a single direction (i.e., axially along the pipe). Such a wave is reflected from damage, and if the pipe geometry is simple, signal interpretation can be straightforward. In contrast, guided waves in plate-like structures are inherently two dimensional. These waves can also travel long distances, but signals are almost always very complicated for even simple structures because of the combined effects of multiple modes, multiple propagation directions, reflections from boundaries, and scattering from structural features [3]. This signal complexity is one of the major impediments to implementation of guided wave methods for nondestructive evaluation (NDE).

Several strategies have been developed in an attempt to overcome signal complexity issues and enable guided wave NDE in plates. One of these, called wavefield imaging, is to record received signals over a dense two dimensional grid using a single transducer source. Another strategy is that of baseline subtraction whereby baseline data are recorded from the undamaged structure and are subsequently subtracted from current signals of interest. This paper reviews methods and presents recent results based upon these two strategies.

2. Wavefield Imaging

The term "wavefield imaging" refers to acquiring full acoustic wavefield data over an area of the exposed part surface for a stationary source and multiple receiver locations. Implementation is typically via a scanned laser vibrometer (SLV) or a scanned air-coupled ultrasonic transducer (SAUT). Results shown here are wavefield data that were acquired from an aluminum plate with various structural discontinuities and artificial defects using an SAUT on a scanning stage. Wave sources were piezoelectric transducers permanently mounted on the specimen that were elements of a permanently attached sparse array. As shown in Figure 1, wavefield images clearly show details of guided waves as they propagate outward from the source, reflect from specimen boundaries, and scatter from discontinuities within the structure. Distinct S_0 and A_0 Lamb incident waves are directly visible on these constant time snapshots of the captured wavefield. However, as can be seen in the figure, the waves propagating outward from the source and reflected from boundaries obscure the weaker scattered waves from holes (H1, H2 and H3) and a second transducer (T6).

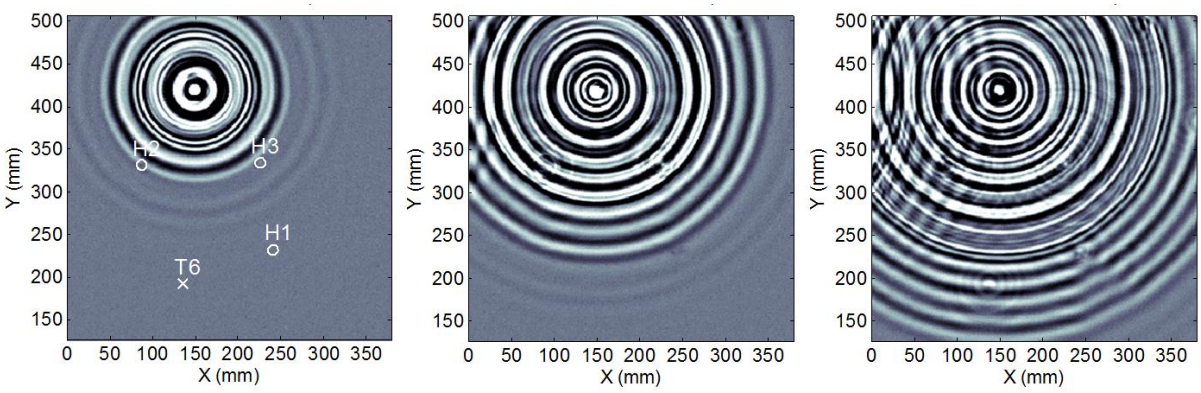

FIGURE 1. Acoustic wavefield images at propagation times of 30, 50 and 70 μs for transmitting on the transducer at (X=150 mm, Y=420 mm). Hole and transducer locations are shown on the 30 μs images, and scattering from these locations is observable on the later time images.

To facilitate analysis of the weaker scattered waves, source waves are removed from the wavefield data using both time and frequency domain methods [4,5]. Figure 2(a) shows a snapshot of a zoomed wavefield image that includes the incident wave and the wave scattered from a hole. Figure 2(b) shows the same image after the incident wave has been partially removed using an adaptive time domain subtraction method. Figure 2(c) shows the same image after the forward propagating wave has been removed by filtering in the $\omega - k_r$ domain. Both methods are effective at removing the incident wave, but also remove part of the scattered wave.

Results from the two methods are fused to obtain more complete information about the scattered wavefields. Figure 3 shows polar representations of the resulting scattered fields, first from a through hole, then the hole with a corner notch, and finally the hole with a through notch; the motivation is to simulate a growing crack. Plots are shown for source waves incident on the notch from two directions, one toward the side of the notch (transducer T1, top row) and the other toward the end of the notch (transducer T6, bottom row). The directional characteristics of the scatterer with respect to the source wave direction are evident along with the varying degrees of mode conversion as the symmetry changes. These

polar plots of the wavefields scattered from two incident wave orientations illustrate one method for experimentally obtaining quantitative flaw scattering characteristics without using damage-free baseline data. Additional details may be found in [6].

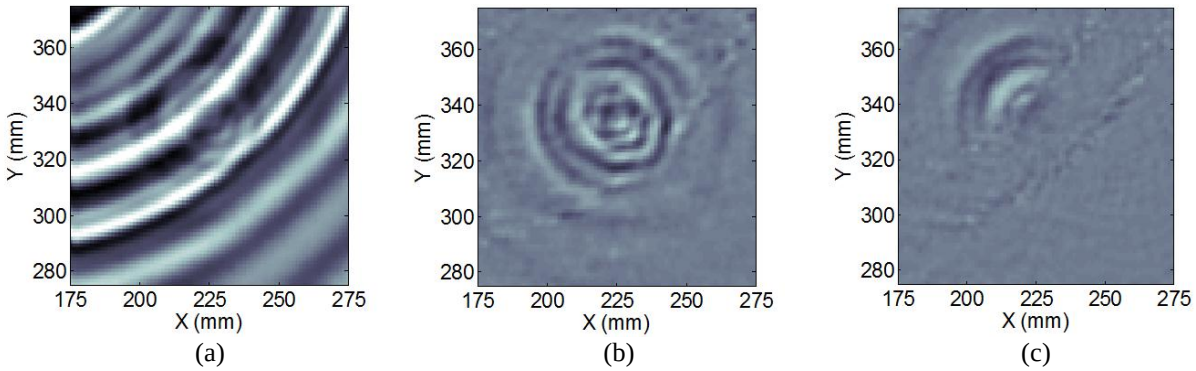

FIGURE 2. Analysis of waveforms in a region around Hole H3 where data were windowed in space over the zoomed region, in time from 0 to 50.6 μs, and in frequency from 0.2 MHz to 0.3 MHz. Snapshots of (a) the original wavefield, (b) after application of the time domain source removal method, and (c) after removing the out-going waves in the $\omega - k_r$ domain (applied to the original wavefield).

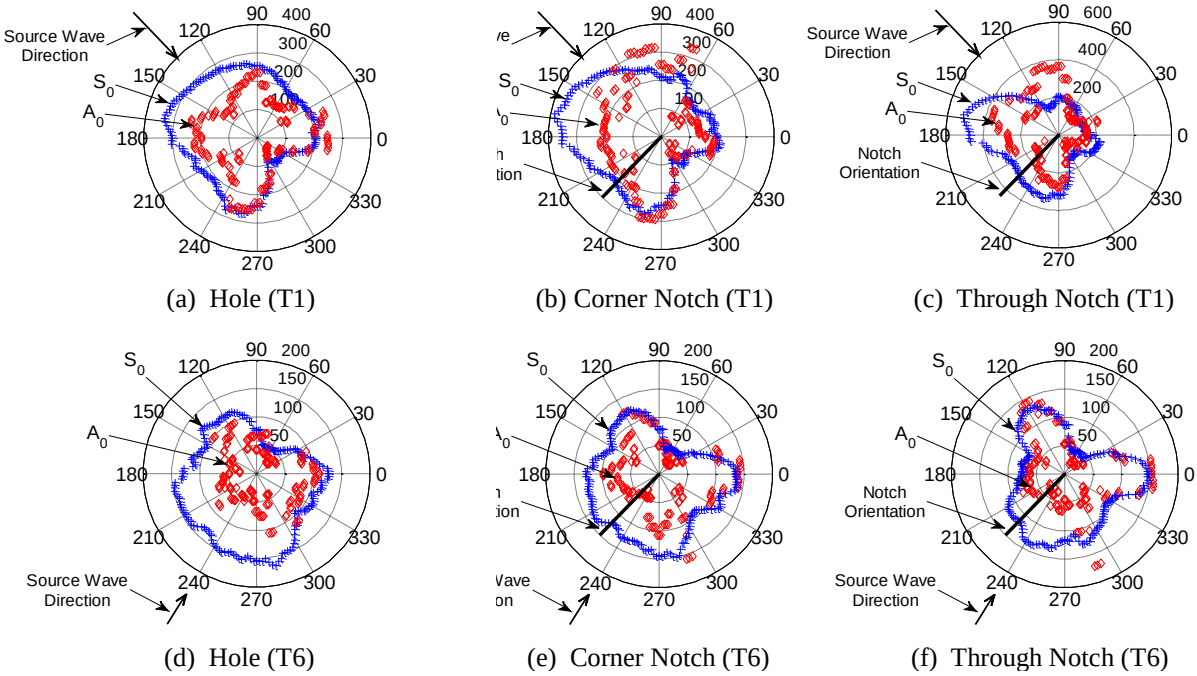

FIGURE 3. Scattered wavefields for hole H3 after combining results from the time domain and the $\omega - k_r$ domain methods to remove the incident wave. (a,b,c) Polar plots of S_0 and A_0 wave mode amplitudes for an incident wave direction of about 135° (approximately broadside to the notch). (d,e,f) Polar plots of S_0 and A_0 wave mode amplitudes for an incident wave direction of about 240° (approximately end-on to the notch).

3. Spatially Distributed Guided Wave Arrays

Spatially distributed arrays consist of individual piezoelectric transducers that are sparsely distributed over a region of interest. These types of arrays are being considered by a number of researchers for *in situ* NDE [7-9], also referred to as structural health monitoring (SHM).

The transducers, which are Lead Zirconate Titanate (PZT) discs, are permanently attached to the structure, and each one can act as either transmitter or receiver of guided elastic waves. The focus of the research activities in this general area has been to develop algorithms to enable detection, localization and characteriation of structural damage based upon changes in recorded guided wave signals.

3.1 Guided wave imaging algorithms

Several imaging algorithms have been implemented for localizing damage in plate-like structures. Delay-and-sum (DAS) type algorithms such as were used in [7-9] can be effective for damage localization, but there are typically significant imaging artifacts. The MVDR (minimum variance distortionless response) adaptive algorithm, which is essentially delay-and-sum imaging with adaptive weights, can provide significant reduction of artifacts but requires knowledge of scattering characteristics [10,11]. Both of these algorithms are applied to the differenced, or residual, signals of a sparse array where baseline signals are subtracted from current signals. In essence, the signal changes are imaged. This subtraction is advantageous for a sparse array because, unlike a compact linear or circular array that relies upon backscattered waves, damage can be introduced in between array elements, and forward scattered signals cannot be separated from the direct arrivals by simple time windowing. Both DAS and MVDR imaging can be performed on either envelope-detected signals or raw (RF) waveforms. Figure 4 shows imaging results for a 6 mm drilled through-hole in an aluminum plate, and illustrates the improvement obtained when using MVDR compared to DAS. Imaging artifacts are suppressed by about 10 dB going from DAS to MVDR using envelope-detected signals, and there is a significant improvement in resolution when using phase information (i.e., imaging with the RF signals).

FIGURE 4. Images from experimental data for a 6 mm diameter through hole. (a) Delay-and-sum imaging with envelope data (10 dB color scale), (b) MVDR imaging with envelope data (20 dB color scale), and (c) MVDR imaging with RF data (20 dB color scale, note zoomed image around scatterer). The open circles are the transducer locations, and the "+" is the location of the scatterer.

The significance of MVDR imaging is that it provides considerably improved results as compared to DAS imaging but with only a modest increase in the computational burden. For some cases, it is also less sensitive to signal-baseline mismatch caused by changes in operational or environmental conditions.

A new imaging algorithm, referred to here as Sparse Reconstruction (SR), was developed to utilize the *a priori* information that damage is sparse. The DAS and MVDR algorithms are not able to take this information into account, which leads to imaging artifacts. The idea of

the SR method is to select pixel values that provide a balance between explaining the data and being spatially sparse. This is accomplished here by using basis pursuit denoising [12] combined with a reasonable model of the guided wave propagation and scattering in the plate. Experimental results are shown in Figure 5 for one and two glued-on masses, which act as scatterers of guided waves and thus simulate damage. What is noteworthy is the complete lack of imaging artifacts away from the actual scattering sites, which is a direct result of the sparsity assumption.

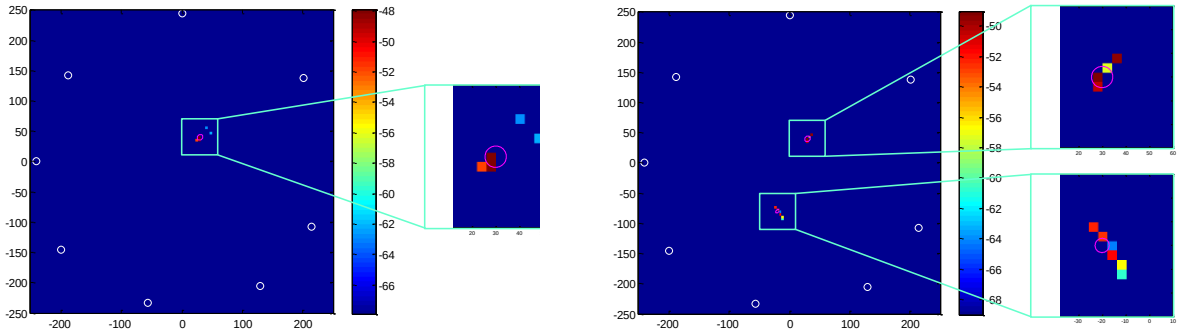

(a) (b)

FIGURE 5. SR images from experimental data for glued-on masses. (a) Single scatterer and (b) two scatterers. Images are shown on a 20 dB color scale; note zoomed views around scatterers. The white open circles are the transducer locations, and the red open circles are the locations of the scatterers.

Development of the SR method is significant because it illustrates how sparsity of damage can be effectively incorporated into imaging of scatterers. Experimental results shown here are limited, and future work needs to consider more realistic structures and damage. Additional information can be found in [13].

3.2 Damage characterization via guided wave imaging

The MVDR method requires that the expected scattering pattern be known (or estimated) prior to imaging, which can be problematic. On the other hand, if several types of scatterers are possible and their scattering patterns are known, MVDR has the advantage of being able to not only locate the scatterers but to characterize them. This idea is illustrated using data recorded from two different notches cut in an aluminum plate. A 15 mm long notch oriented at +45° was located in the lower left corner of the plate, and a similar notch oriented at -45° was located near the center of the plate. These notches, like cracks, are highly directional scatterers, and thus the two notches at the two different orientations scatter the guided waves quite differently.

Figure 6(a) shows the image generated of the +45° notch using the correct scattering pattern, whereas Figure 6(b) is the corresponding image on the same scale but created using the scattering pattern of a notch at 90°. Clearly the response is almost 20 dB lower in amplitude when the incorrect scattering pattern is used for imaging. Figure 6(c) shows the maximum response for both notches as a function of the orientation angle of the assumed scattering pattern. The peak locations of each curve agree well with the actual notch orientations. These results indicate that small scatterers can be characterized using a sparse array if their scattering characteristics are known and are sufficiently different. This idea is much different than traditional methods for characterizing scatterers using many measurements to directly

trace out the scattering pattern. Most importantly, it points the way to practical, *in situ* damage characterization using a very small number of transducers. Additional results can be found in [14].

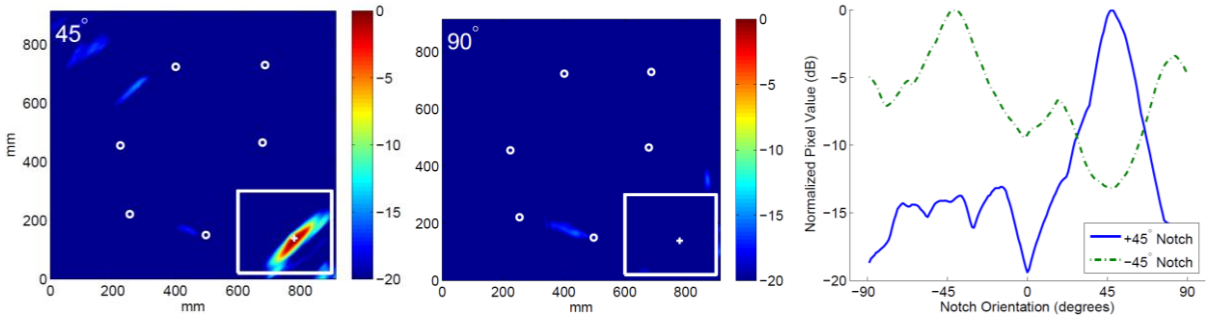

FIGURE 6. Example of damage characterization via MVDR imaging. (a) MVDR image of a +45° notch using the correct scattering pattern. (b) MVDR image of the same notch but using an incorrect scattering pattern. (c) Maximum MVDR image amplitudes for both notches assuming scattering patterns corresponding to notch orientations of -90° to +90°.

3.3 Temperature effects

Variable operational and environmental conditions can adversely affect the performance of SHM systems by causing changes in guided wave signals that may either be mistaken for damage or mask damage. The three most common such conditions are temperature, stresses, and surface wetting; temperature is perhaps the most important because very small changes in temperature can significantly affect both detection and localization of damage.

The basic idea for most, if not all, temperature compensation methods is to (1) record baseline signals at a range of temperatures, (2) find the baseline signal that best matches the current signal of interest, and (3) adjust this signal to better match the current signal; refer to [9], [15] and [16] for details and examples. The first two steps are usually referred to as optimal baseline selection (OBS), and the last by baseline signal stretch (BSS) because signal stretching (with slight time shifts) is the usual method to achieve matching. This basic method was improved upon in several significant ways as summarized in Table 1:

TABLE 1. Summary of changes to the OBS+BSS temperature compensation method.

Original Method	New Method
1. Stretch implemented in the frequency domain	1. Stretch implemented in the time domain
2. Stretch/shift algorithm: a. Stretch computed from lags of short time cross correlation plotted at time window centers b. Shift determined by cross correlation of entire stretched waveforms	2. Stretch/shift algorithm: a. Stretch computed from lags of short time cross correlation plotted at center of energy b. Shift is y-intercept of lags vs. time
3. Same baseline set selected for all pairs	3. Individual baseline selected for each pair
4. Single baseline used to construct matched signal	4. Weighted average of two baselines used to construct matched signal

These changes resulted in significant improvement in temperature compensation as measured by the detection margin – the dB difference in the residual signal before and after damage. Table 2 is a tabulation of improvement for five representative transducer pairs from a specific aluminum plate experiment. Note that the new method was able to achieve significantly better performance while using less data (smaller time window and lower sampling frequency). More details are found in [17].

TABLE 2. Summary of detection margins for original and new methods of temperature compensation.

Transducer Pair	Detection Margin (dB)		
	Original Method		New Method
	4000 μs, 25 MHz	1000 μs, 5 MHz	1000 μs, 5 MHz
1-3	4.30	1.30	7.06
2-3	3.10	2.48	6.83
3-4	4.80	1.82	6.16
3-5	1.02	-2.80	4.09
3-6	3.49	1.14	3.91

3.4 Loading effects

Applied loads cause similar effects as temperature because, like temperature, loads change both specimen dimensions and wave speeds. An important difference is that loads are generally anisotropic, which prohibits the BSS method from being used. To investigate loading effects, an aluminum plate specimen with a central hole was fatigued. Data were recorded as a function of load before the hole was drilled, after the hole was drilled, and at intervals thereafter as a function of fatigue life.

Figure 7 illustrates the effects of matched loads on a fatigue crack about 5 mm in length. Figures 7(a), (b) and (c) correspond to loads of 0, 57.5 and 115 MPa, respectively. It is clear that the main effect of the load is to open the crack. It is not detected at zero load, but as the load increases the crack opens and becomes increasingly evident.

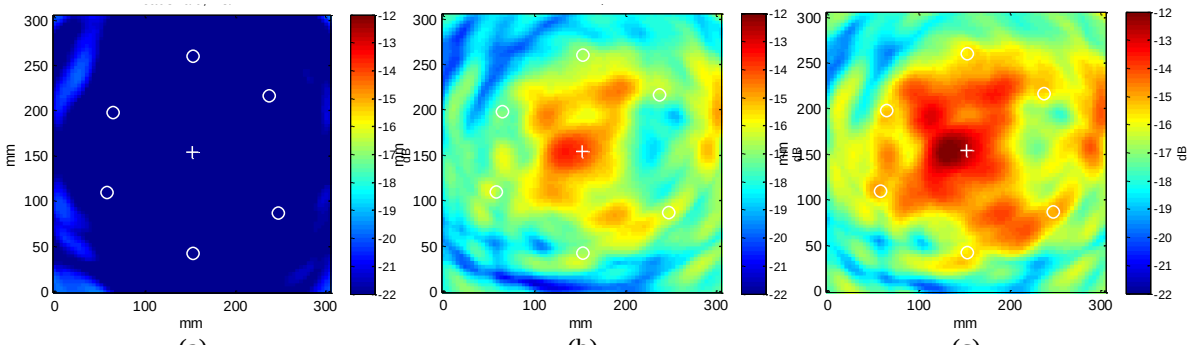

FIGURE 7. Images constructed between pre-crack baseline signals and current signals recorded after growth of a ~5 mm fatigue crack. Both signals were recorded at the load indicated. (a) 0 MPa, (b) 57.5 MPa, and (c) 115 MPa. Images are shown on the same 10 dB color scale normalized to the overall peak value.

Figure 8 illustrates the effects of mismatched loads on the same fatigue crack. Signals from the crack were recorded at the maximum load of 115 MPa, whereas the baseline signals were recorded at variable but mismatched loads. Since the crack is fully opened for all three images, the main effect of the varying load of the baseline signals is to introduce imaging artifacts. For the images of Figure 8(a) and (b), the artifacts are as large as or larger than the crack, and thus the crack is not detectable. For Figure 8(c), where the mismatch is smaller, the image is only slightly degraded from that of Figure 7(c) and the crack is clearly detected.

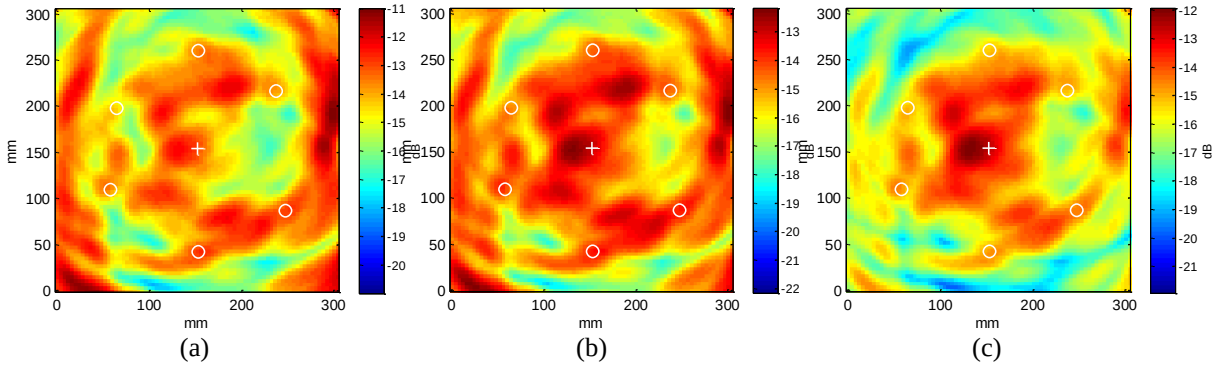

FIGURE 8. Images constructed between pre-crack baseline signals and current signals recorded after growth of a ~5 mm fatigue crack. Current signals were recorded at the maximum load (115 MPa), and baseline signals were recorded at the load indicated. (a) 0 MPa, (b) 46 MPa, and (c) 92 MPa. Images are shown on separate 10 dB color scales with each normalized to its peak value.

These results illustrate the importance of both matched loads and loads sufficient to open cracks. They have also motivated development of load-differential imaging methods where baselines are recorded at one load and current signals at a slightly higher load but at the same damage state [18]. Figure 9 shows three sets of images generated by differential loads of 11.5 MPa. For the top row, there are no visible cracks, for the middle row there is a single 8 mm long crack, and for the bottom row there are two cracks of lengths 20 mm and 12 mm, one on each side of the hole. These images clearly show the cracks opening with load and did not use a damage-free baseline.

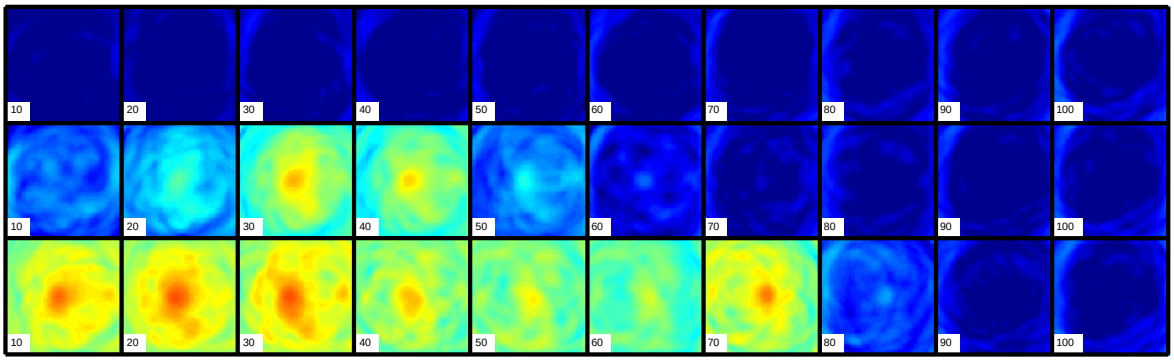

FIGURE 9. Load-differential images. Top row: no visible cracks. Middle row: single 8 mm long crack. Bottom row: two cracks of lengths 20 mm and 12 mm, one on each side of the hole. The differential loads increase from 0-10% to 90-100% from left to right, and the color scale is 30 dB.

4. Concluding Remarks

Results shown here illustrate both the challenges and the opportunities for using ultrasonic guided waves for both conventional and *in situ* NDE. Wavefield imaging has the potential to characterize defects by quantifying the full wavefield scattered from a flaw. Sparse, or spatially distributed, arrays have potential for *in situ* detection, localization and characterization of damage by monitoring changes in received signals. In general, the effects of variable operational and environmental conditions must be considered because the interaction of guided waves with boundaries makes them more sensitive to these variations than bulk waves.

Acknowledgements

This work reported here would not have been possible without the support and direct contributions of Dr. Sang Jun Lee, Dr. James S. Hall, Mr. Navneet Gandhi, Mr. Xin Chen and Mr. Ross Levine. The authors also gratefully acknowledge the financial support of the Air Force Office of Scientific Research, Grant No. FA9550-08-1-0241, and the Air Force Research Laboratory, Contract No. FA8650-09-C-5206.

References

1. P. Cawley, M. J. S. Lowe, D. N. Alleyne, B. Pavlakovic, and P. Wilcox, "Practical long range guided wave testing: Applications to pipes and rail," *Materials Evaluation*, **61**(1), pp. 66-74, 2003.
2. www.guided-ultrasonics.com
3. R. P. Dalton, P. Cawley and M. J. S. Lowe, "The potential of guided waves for monitoring of large areas of metallic aircraft fuselage structure," *Journal of Nondestructive Evaluation*, **20**(1), pp. 29-46, 2001.
4. Z. M. Master, T. E. Michaels and J. E. Michaels, "Incident wave removal for enhancement of defects in acoustic wavefield images," *Review of Progress in QNDE*, **26A**, D. O. Thompson and D. E. Chimenti (Eds.), AIP, pp. 665-672, 2007.
5. T. E. Michaels, J. E. Michaels and M. Ruzzene, "Frequency-wavenumber domain analysis of guided wavefields," *Ultrasonics*, **51**, pp. 452-466, 2011.
6. T. E. Michaels, M. Ruzzene and J. E. Michaels, "Frequency-wavenumber domain methods for analysis of incident and scattered guided waves," *Proceedings of SPIE*, T. Kundu (Ed.), SPIE, **7295**, pp. 729513:1-12, 2009.
7. C. H. Wang, J. T. Rose, and F.-K. Chang, "A synthetic time-reversal imaging method for structural health monitoring," *Smart Materials and Structures*, **13**(2), pp. 415-423, 2004.
8. J. E. Michaels, "Detection, localization and characterization of damage in plates with an *in situ* array of spatially distributed ultrasonic sensors," *Smart Materials and Structures*, **17**, 035035 (15pp), 2008.
9. T. Clarke, P. Cawley. P. D. Wilcox and A. J. Croxford, " Evaluation of the damage detection capability of a sparse-array guided-wave SHM system applied to a complex structure under varying thermal conditions," *IEEE Transactions on Ultrasonics, Ferrolectrics, and Frequency Control*, **56**(12), pp. 2666-2678, 2009.

10. J. S. Hall and J. E. Michaels, "Minimum variance ultrasonic imaging applied to an *in situ* sparse guided wave array," *IEEE Transactions on Ultrasonics, Ferroelectrics, and Frequency Control*, **57**(10), pp. 2311-2323, 2010.
11. J. S. Hall and J. E. Michaels, "Computational efficiency of ultrasonic guided wave imaging," *IEEE Transactions on Ultrasonics, Ferroelectrics, and Frequency Control*, **58**(1), pp. 244-248, 2011.
12. S. S. Chen, D. L. Donoho, and M. A. Saunders, "Atomic decomposition by basis pursuit," *SIAM Journal of Scientific Computing*, **20**(1), pp. 33-61, 1999.
13. R. M. Levine, J. E. Michaels and T. E. Michaels, "Guided wave localization of damage via sparse reconstruction," *Review of Progress in QNDE*, D. O. Thompson and D. E. Chimenti (Eds.), AIP, **31**, to appear 2012.
14. J. S. Hall, P. Fromme and J. E. Michaels, "Ultrasonic guided wave imaging for damage characterization," *2011 Aircraft Airworthiness & Sustainment Conference*, San Diego, CA, April 18-21, 2011 (available online at http://www.airworthiness.com).
15. Y. Lu and J. E. Michaels, "A methodology for structural health monitoring with diffuse ultrasonic waves in the presence of temperature variations," *Ultrasonics*, **43**, pp. 717-731, 2005.
16. A. J. Croxford, J. Moll, P. D. Wilcox and J. E. Michaels, "Efficient temperature compensation strategies for guided wave structural health monitoring," *Ultrasonics*, **50**, pp. 517-528, 2010.
17. Z. Lu, S. J. Lee, J. E. Michaels and T. E. Michaels, "On the optimization of temperature compensation for guided wave structural health monitoring," *Review of Progress in QNDE*, D. O. Thompson and D. E. Chimenti (Eds.), AIP, **29B**, pp. 1860-1867, 2010.
18. X. Chen, S. J. Lee, J. E. Michaels and T. E. Michaels, "Load-differential features for automated detection of fatigue cracks using guided waves," *Review of Progress in QNDE*, **31**, D. O. Thompson and D. E. Chimenti (Eds.), AIP, expected 2012.